archives
of thermodynamics
Vol. **39**(2018), No. 2, 123–146
DOI: 10.1515/aoter-2018-0015

Pressure drop related to flow maldistribution in a model minichannel plate heat exchanger

MICHAŁ KLUGMANN
PAWEŁ DABROWSKI*
DARIUSZ MIKIELEWICZ

Gdańsk University of Technology, Narutowicza 11/12, 80-233 Gdańsk, Poland

Abstract The paper describes issues related to pressure drop that accompanies the phenomenon of maldistribution of working fluid between the channels of a model minichannel plate heat exchanger. The research concerns a single exchanger's plate containing 51 (in every geometry) parallel rectangular minichannels of hydraulic diameters 461 μm, 571 μm, 750 μm, and 823 μm. In addition, more complex geometry has been investigated, equipped with additional diagonal channels (so called extended geometry). The moment of the liquid phase transition through the heat exchanger was recorded at the flow rates ranging from 0.83 g/s to 13.33 g/s in the inlet manifold. The paper discusses the total pressure drop as a function of the flow rate and the characteristic dimension of minichannels, as well as the pressure drop as a function of the time of the fluid passage through the main part of the measuring section in which measurements were done. The resulting profiles correlate with the images of the flow distribution between channels recorded using the fast shutter speed camera, that allows to draw a further conclusions about the specifics of the maldistribution process. The impact of the total pressure drop on the actual range of optimum operating conditions of the heat exchanger was analyzed.

Keywords: Pressure drop; Transient flow; Minichannel plate heat exchanger; Flow maldistribution

*Corresponding Author. Email: pawel.dabrowski@pg.edu.pl

Nomenclature

A	–	surface area, m^2
Bo	–	Bond number, $Bo = g(\rho_L - \rho_g)(D_h/2)/\sigma$
D_h	–	hydraulic diameter, m
G	–	mass flux, $G = \dot{m}/A$, kg/m^2s
h	–	convective heat transfer coefficient, W/m^2K
k_f	–	thermal conductivity, W/mK
L	–	channel length, m
$\dot{m}$	–	mass flow rate, kg/s
Nu_∞	–	Nusselt number for fully-developed temperature profile
P_w	–	wetted perimeter, m
Re	–	Reynolds number, $Re = uD_h/\nu$
u	–	mean value in microchannel velocities, m/s
We	–	Weber number, $We = G^2 D_h/(\rho_L \sigma)$

Greek symbols

ΔP	–	pressure drop, Pa
λ	–	friction factor
ν	–	kinematic viscosity, m^2/s
ρ	–	density, kg/m^3
σ	–	surface tension of liquid, N/m

1 Introduction

Majority of the technology sectors are endeavoring to miniaturization with simultaneous performance improvement. The sizes of electronic equipment are becoming smaller while the clock frequency, hence the amount of heat produced are becoming higher. That causes an increase of heat flux which is necessary to dissipate from the surface. For example, the average value of heat flux generated by computer processors ranges from 2 to 4.5 MW/m^2 (up to 45 MW/m^2 locally); whereas for insulated gate bipolar transistors (IGBT) – from 6.5 to 50 MW/m^2. Hence, there is a need to focus on modern kinds of highly compact and high efficiency heat exchangers design and to maximize the heat transfer [1]. Unfortunately, the cost for improving heat exchanger parameters, both in terms of performance as well as compactness, is always an increase of pressure drop [2]. In the case of the flow forced by the pump this involves the necessity of consideration the energy expenditure and the size of the pump itself. In the case of natural circulation (e.g., in thermosiphon applications) the situation is more radical because too much flow resistance can completely prevent the device from running. Hence, the attempts of applying minichannel and minigap geometries to the construction of highly efficient, compact heat exchang-

ers requires a special focus on this problem on equal footing with other important issues (flow instabilities, maldistribution, impact of fluid impurities, that can easily block minichannels). This paper considers a pressure drop in two ways: a) total pressure drop at a steady flow of water as an effect of total flow resistance; b) local pressure drop as a function of time on the main part of test section (inlet manifold – minichannels – outlet manifold). This is – *de facto* – an increase in pressure drop caused by a change of working medium flowing through the section (air-water). The course of this change is directly related to the process of medium distribution (or maldistribution) in the exchanger and, therefore, requires analysis in conjunction with this phenomenon.

2 State of the art

Tuckerman and Pease clearly demonstrated, about four decades ago, that convective heat transfer coefficient strictly depends on hydraulic diameter of the channel [3]

$$h = \frac{k_f \mathrm{Nu}_\infty}{D_h} \,, \tag{1}$$

where hydraulic diameter can be calculated from [4]

$$D_h = \frac{4A}{P}_w \,. \tag{2}$$

The smaller hydraulic diameter, the higher the convective heat transfer coefficient. This remark introduces new generation of heat exchangers i.e. minichannel heat exchangers.

Micro- and minichannels are different from the conventional channels in terms of channel hydraulic diameters. Ranges of hydraulic diameters proposed by [5] are as follows: $D_h > 6$ mm for macrochannels, 1 mm $< D_h < 6$ mm for compact channels, 0.1 mm $< D_h < 1$ mm for mesochannels, and 1 μm $< D_h < 100$ μm for microchannels. Different classification was made in [6], i.e., channels can be defined as conventional when $D_h > 3$ mm, mini when 0.2 mm $< D_h < 3$ mm, and micro when 10 mm $< D_h < 200$ μm.

Mini- or microchannel heat exchangers are widely used in many industries, i.e., power industry (water cooled turbine blades, rocket nozzle cooling, fusion reactor blanket cooling, domestic micro combined heat and power (micro-CHP) [7–11], electronics industry (microprocessors, light-emitting diode (LED) cooling) [12–14], avionics industry (avionics cooling)

[15], space industry (cooling of satellite electronics) [16], solar industry (solar, photovoltaic panels) [17,18], automotive industry (multiport condensers) [19], chemical and biological industry [20–22], refrigeration industry (microfin tubes in residential cooling, heat pumps) [23,24] and cryogenic industry (heat exchangers for hydrogen production systems) [25]. Kandlikar [26] reported that microchannels may provide a heat flux dissipation ratio of up to 103 W/cm^2.

Mini- and microdiameter of channels causes a low mass flux of fluid that is able to flow through it and small total heat flux that can be dissipated from cooled surface as a result. That is a reason for application of many parallel minichannels with common inlet and outlet manifold in minichannel heat exchangers. Total cross section of minichannel package can be relatively large despite the small diameter of individual channels. However, the surface of the walls wetted by the liquid is also large. In addition, the phenomena characteristic for the flow in the minichannels are occurring. All this makes the flow resistances and, consequently, pressure drops a particularly important work parameters of minichannel heat exchangers.

Linear flow resistances are described by the Darcy-Weisbach equation

$$\Delta P = \lambda \frac{L}{D_h} \frac{\rho u^2}{2} \,. \tag{3}$$

It follows that the smaller the hydraulic diameter and the greater the flow velocity (i.e., the greater the flow of the medium), the greater is resulting pressure drop. Dimensions of mini- and microchannels imply small volume flows so that the pressure drop can be compensable by the hydraulic pump. Therefore, when deciding on microchannel heat exchangers, it should be borne in mind that the volumetric flow rate of the medium should be small. Hence, it would be a good idea to use microchannels in thermosiphon systems that operate on the basis of the density difference between fluid at low and high temperatures. In systems where the free convection is used, the flows are small and the microchannel exchangers can bring very good results.

In addition to high pressure drop, another problem in microchannel technology is pressure fluctuations. Qu and Mudawar observed them in a microchannel heat sink. The cooling medium was water, flowing in 21 parallel rectangular microchannels (hydraulic diameter of 349 μm per each). The operating parameters were a mass flow (in range from 134.9 kg/m^{2}s to 400.1 kg/m^{2}s) and the supplied heat flux (in range from 0.004 W/m^2 to 0.013 W/m^2). The authors stated that the described pressure oscilla-

tions can be reduced or eliminated by throttling the flow before the heat exchanger [27].

There are some works that are trying to model the operation of small fin plate heat exchangers. There are among others [28,29]. Authors developed a mathemtical model that enables to predict, with good accuracy, parameters such as pressure and temperature drops at the exit of cold and hot sides of heat exchanger. They showed that there are many parameters that infuence the effectiveness of the plate fin heat exchanger. These parameters can be named as geometrical parameters, properties of the working fluid and operational conditions such as mass flow and pressure drops.

3 Aim of the work

The purpose of the presented research was to find the relationship between the pressure drop and the specified of the flow distribution in the model plate minichannel heat exchange, which was designed and investigated in other aspects earlier [30,31]. Especially important is an attempt to find the relationship between the pressure drop and the presence and nature of flow maldistribution. This is another step in explaining the maldistribution phenomenon itself. Except that, the parameters such as flowrate and the characteristic dimension of minichannels were taken into account. A single exchanger's plate containing of 51 (in every geometry) parallel, rectangular minichannels of hydraulic diameters 461 μm, 571 μm, 750 μm, and 823 μm was submitted to analysis. In addition, the more complex geometry has been investigated, equipped with additional diagonal channels (further called extended geometry). The conditions were adiabatic (without heat exchange). The analysis was related to the moment of the liquid phase transition through the measurement section with the use of water as the working medium. The continuous pressure recording at the inlet to the measuring section was carried out with a frequency of 50 readings per second. At the same time the process was registered with a fast shutter speed camera. These registrations were synchronized so the instantaneous pressure values could be associated with the actual image of the process.

4 Experimental setup and research procedure

The measuring system was built as an open layout. Diagram of experimental rig is shown in Fig. 1. Demineralized and degassed water was supplied to the installation gravitationally using a miniature water tower. It's design (hydrostatic pressure, cross-sections of pipelines) was established to provide a pressure of 5 kPa and up to 16.66 g/s of a flowrate at the 'start point'. Concept of the test section was designed so that it could finally work in the thermosiphon circuit as an evaporator. Also the range of flow parameters for which the measurements were carried out was matched to the nature of thermosiphon's work.

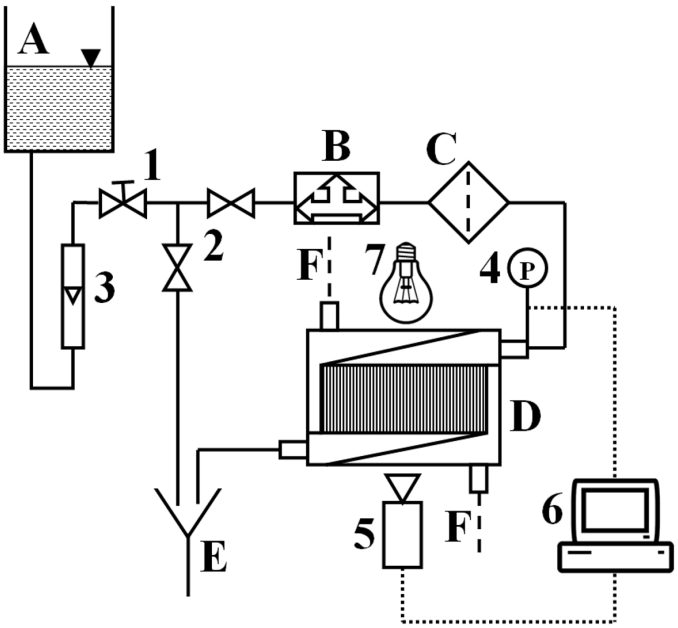

Figure 1: Diagram of experimental rig, elements of the flow system: A – water tank, B – air separation system, C – filter, D – test section, E – outflow, F – section heating/cooling facility; elements of the control and measuring system: 1 – control valve, 2 – cut-off valve, 3 – rotameter, 4 – pressure transducer, 5 – fast shutter speed camera, 6 – synchronization and data acquisition system, 7 – light source.

Pressure measurement was carried out using the ATM.1ST electronic pressure transmitter with a measuring range of 0 to 5 kPa. It was linked to the National Instruments SCXI-1600 measuring interface and LabVIEW engi-

neering software environment. Alternatively, the authors introduced their own unique method of pressure measurement using a U-tube and real-time image analysis performed by dedicated computer software to collect it's measured values. This method (although it still requires a recognition and consideration of additional phenomena) showed unique advantages. To record the fluid distribution in the measuring section a fast-shutter, also known as FullHD speed camera was used (e.g., parameters: resolution 1920×1080, shutter speed in range from 50 to 500 μs, frame rate 50 fps, focal length/small pic. eqiv. of 70 mm). A signal generated by LabVIEW engineering software environment was used to synchronize recordings of individual devices. Volumetric flowrate measurement was carried out with a rotameter with a measuring range of 0 to 8.33 cm^3/s and the elementary scale 0.083 cm^3/s and then mass flow rate was calculated.

In addition, the measurement system has been equipped with a deaeration facility and a filter to remove any particles in the work fluid. Following geometries were tested:

- Basic (Fig. 2): 51 parallel minichannels, width 1 mm, depth 0.3 mm (461 μm), 0.4 mm (571 μm), 0.6 mm (750 μm) and 0.7 mm (823 μm).
- Extended (Fig. 3): 51 parallel minichannels with additional cross-cut channels, width 1 mm, depth 0.4 mm (571 μm).

The experiment was performed at a range of flowrates from 0.83 g/s to 8.33 g/s and, for some cases, additionally at 10 g/s and 13.33 g/s for accurate registration the specifics of pressure drop. No channel blocking phenomena were observed for the flowrate above 8.33 g/s, so there was no need to extend the measurements above this value for all cases. Pressure measurement was done only at the inlet. At the outlet the atmospheric pressure was assumed.

5 Results and discussion

All flow-related parameters are listed in Tab. 1. All obtained results have been referred to the mass flow rate. Table 1 is useful to transform those results if it is need to refer it to the mass flux or various non-dimensional parameters.

From an application perspective, an important information is the total pressure drop in the exchanger, taking into account not only inlet manifold, set of minichannels and outlet manifold but also the entire remaining flow

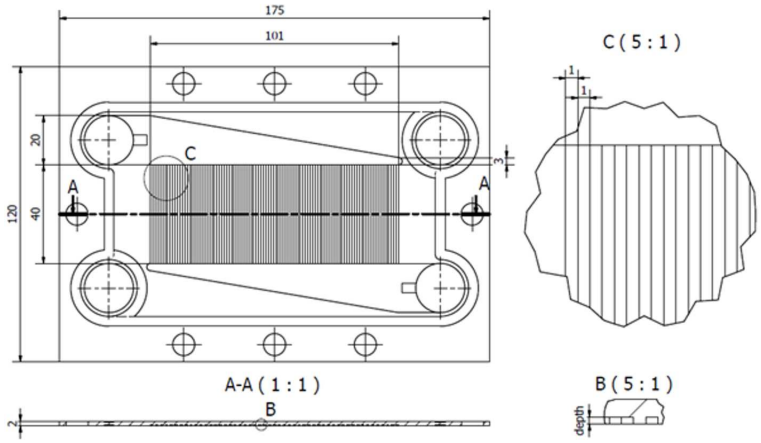

Figure 2: The investigated basic minichannel plate.

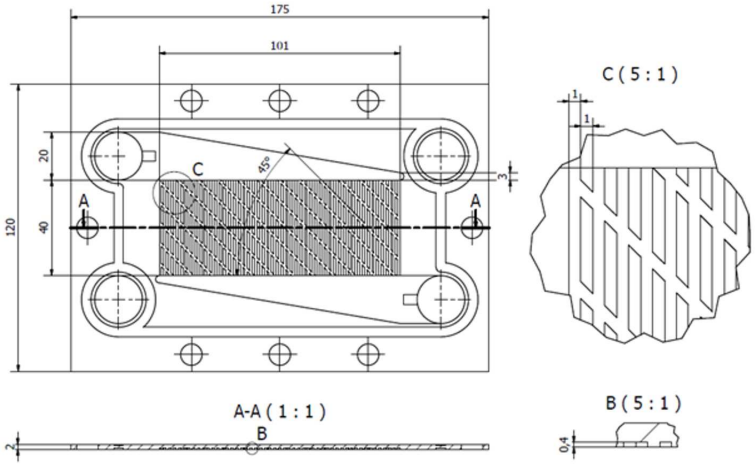

Figure 3: The investigated extended minichannel plate.

system. This approach is shown in Fig. 4. But from the point of view of phenomena in the main structure of the exchanger and, in particular, to find the relationship between the pressure drop and the maldistribution phenomenon, a strictly local pressure drop in a single exchanger's plate structure is important. This is shown in Fig. 5. As can be seen, the curves shape in Fig. 4 correspond to pressure drops in single minichannel plate itself (without hydraulic resistance in valves and the connectors, Fig. 5),

Table 1: Flow-related parameters.

Parameter	$\dot{m}$	G	Re	We		$\dot{m}$	G	Re	We
Unit	g/s	kg/m^{2}s	–	–		g/s	kg/m^{2}s	–	–
$D_h = 461$ μm; Bo = 0.0072	0.90	2991	1376	57	$D_h = 750$ μm; Bo = 0.0189	0.95	1579	1180	26
	1.94	6481	2982	268		1.81	3019	2257	95
	2.59	8641	3976	477		2.68	4459	3334	206
	3.41	11355	5225	823		3.56	5927	4432	364
	4.24	14124	6499	1274		4.32	7201	5384	538
	4.87	16229	7468	1682		5.23	8724	6523	790
	5.88	19608	9023	2455		6.07	10108	7559	1060
	6.61	22045	10144	3103		6.85	11410	8532	1351
	6.98	23263	10705	3456		7.24	12075	9029	1513
	7.53	25091	11546	4020		8.21	13681	10230	1942
$D_h = 571$ μm; Bo = 0.0110	0.71	1786	1018	25	$D_h = 823$ μm; Bo = 0.0228	1.51	2160	1774	53
	1.94	4860	2769	187		2.68	3822	3138	166
	2.64	6605	3763	345		4.00	5716	4693	372
	3.56	8890	5065	625		5.02	7178	5894	587
	4.29	10718	6106	908		5.93	8475	6958	818
	5.15	12878	7337	1311		7.14	10203	8377	1186
	5.65	14124	8047	1577		8.49	12130	9960	1676
	6.51	16284	9278	2096		9.77	13958	11461	2220
	7.06	17655	10059	2464		10.14	14490	11897	2392
	7.89	19732	11242	3078		11.31	16151	13262	2972

in the terms of overall trend. In general, the pressure drop as a function of mass flow rate increase as the mass flow rate increases. This is in line with the accepted state of the knowledge about the flow phenomena. The curves of total pressure drop in the model exchanger (including inlet connector, valves, etc.) are clearly parabolic, what means very strong increase for the higher flowrate values. For the case of pressure drop in main part of the measuring section problem is more subtle. It is evident that the course of the curves is changing above the flowrate of 6.5 g/s. It became more 'flat'. It has a relationship with the critical flowrate below which the maldistribution occurs and intensifies for these specific geometries. This is the same order of magnitude (in range from 5 to 8 g/s, depends from the minichannel depth). After a certain range of gentle run there is a strong

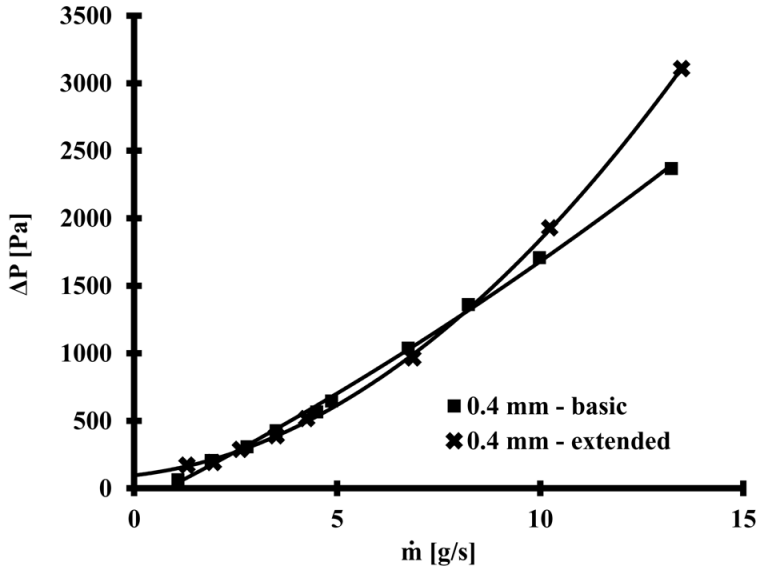

Figure 4: Total pressure drop in the model exchanger (including, among others, inlet connector) as a function of mass flow rate for basic and extended geometry.

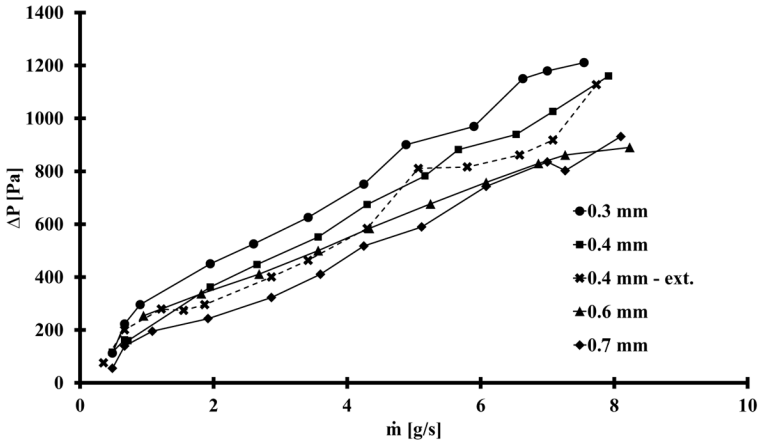

Figure 5: Pressure drop as a function of mass flow rate for various minichannels depth for a main part of test section (inlet manifold – set of minichannels – outlet manifold).

increase in pressure drop resulting from the general parabolic shape of the curve. This confirms the existence of a limited area of optimum working conditions that is available for this type of exchanger.

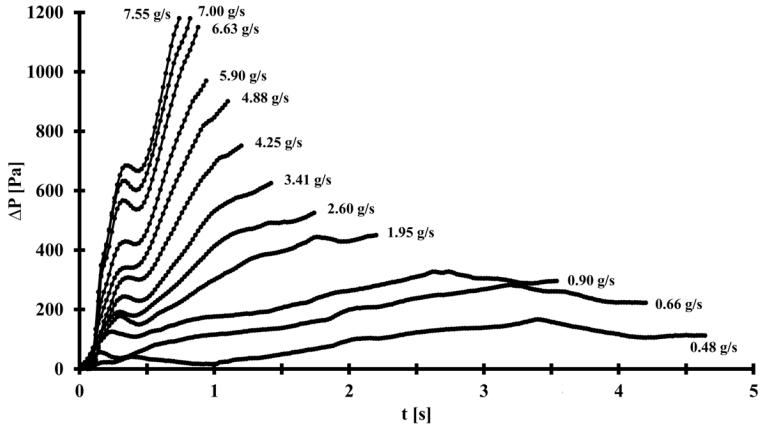

Figure 6: Local pressure drop as a function of a section filling time for several flowrates: basic geometry, depth of 0.3 mm.

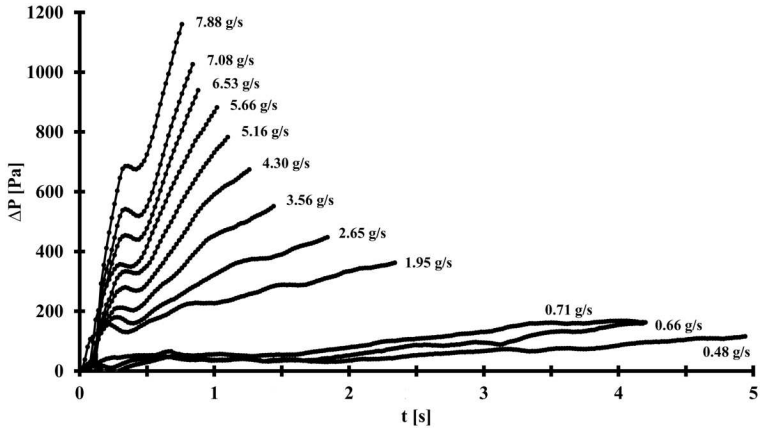

Figure 7: Local pressure drop as a function of a section filling time for several flowrates: basic geometry, depth of 0.4 mm.

As can be seen in Fig. 5, for the flowrate ranging from 5 g/s to 8 g/s the pressure drops in the main part of the test section are in the range from 600 Pa to 1250 Pa, depends on the hydraulic diameter of channels. The total pressure drop for the entire exchanger (including inlet connector) was up to 4.5 kPa. The introduction of additional cross-cut channels (the complication of geometry) – as expected – resulted in a further increase in flow resistance at higher flow rates (above 8 g/s). The reason for this is a flow turbulence caused by a much more complex flow structure. The profiles of

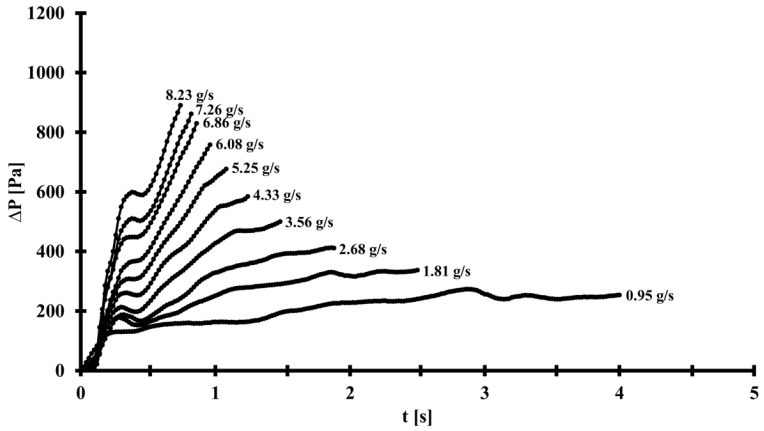

Figure 8: Local pressure drop as a function of a section filling time for several flowrates: basic geometry, depth of 0.6 mm.

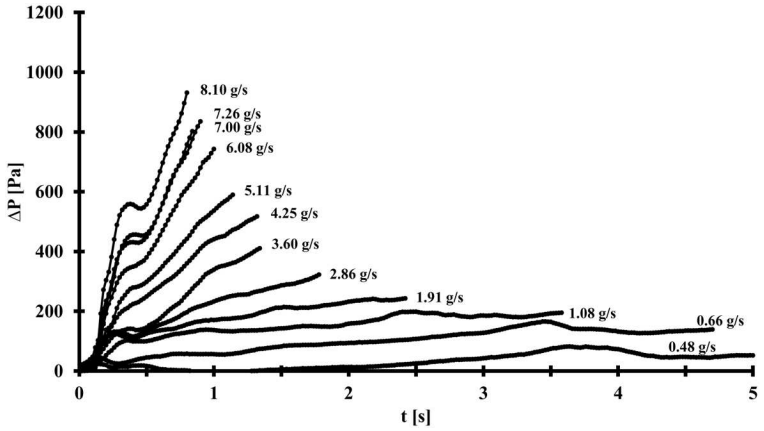

Figure 9: Local pressure drop as a function of a section filling time for several flowrates: basic geometry, depth of 0.7 mm.

a local pressure drop as a function of time of the liquid phase transition through the main section part are very specific and can be related to the broader specificity of the flow character in the particular geometry.

It is visible in Figs. 6–9 that the shapes of the pressure drop curves are practically the same for every minichannel depth. The duration of the processes is also very similar. The only difference is the quantitative difference in pressure values, especially visible for maximum pressure drops for the highest flowrates. The extended geometry works a bit different, as can be

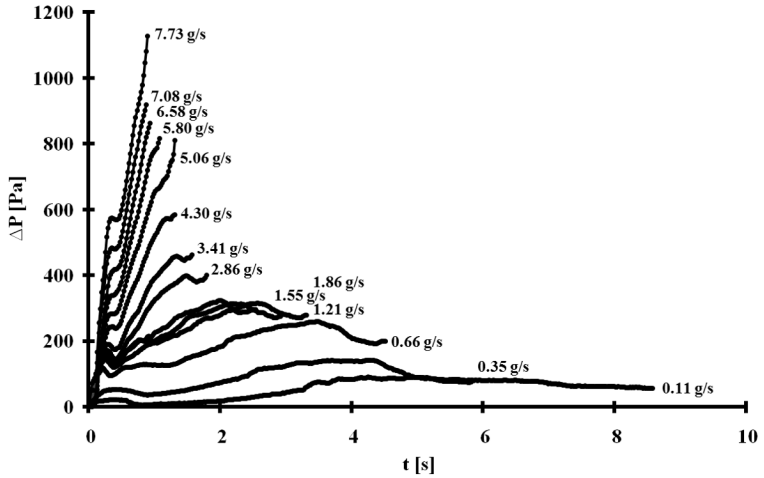

Figure 10: Local pressure drop as a function of a section filling time for several flowrates: extended geometry, depth of 0.4 mm.

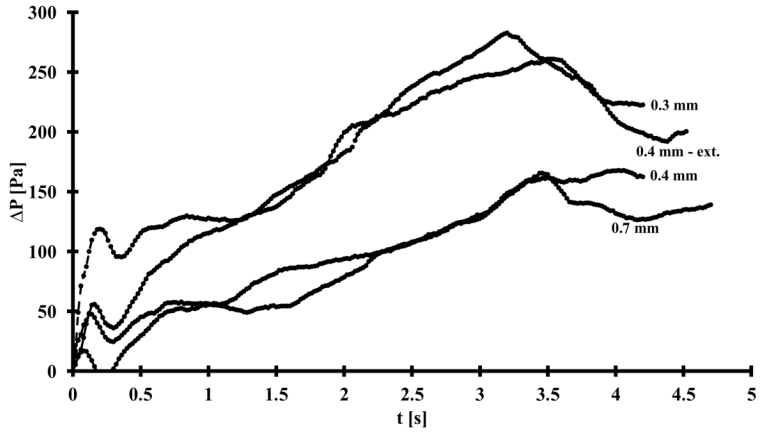

Figure 11: Local pressure drop as a function of a section filling time for several minichannel depths and average flowrate of 0.7 g/s.

seen in Fig. 10. Duration of process is longer.

Figure 11 shows the comparison of pressure drop curves for the lower flow rate (average value about 0.7 g/s). Figures 12 and 13 show the same comparison for flowrate of 1.91 g/s and 3.56 g/s respectively. Figure 14 shows the comparison of pressure drop curves for the upper measured flowrate (average value 7 g/s), which gives a tenfold difference in

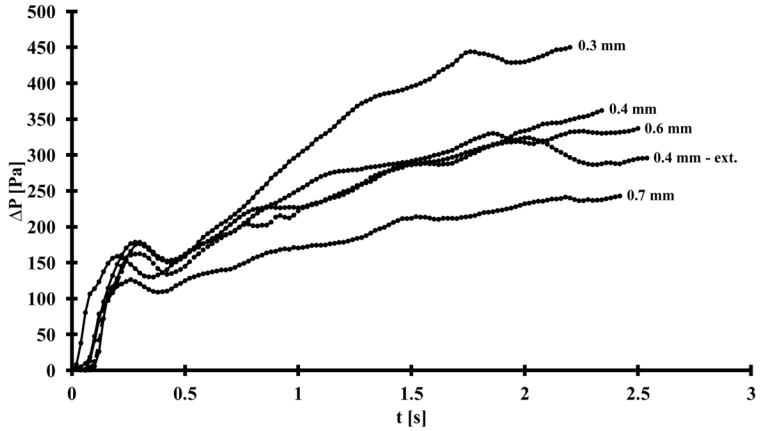

Figure 12: Local pressure drop as a function of a section filling time for several minichannel depths and average flowrate of 1.91 g/s.

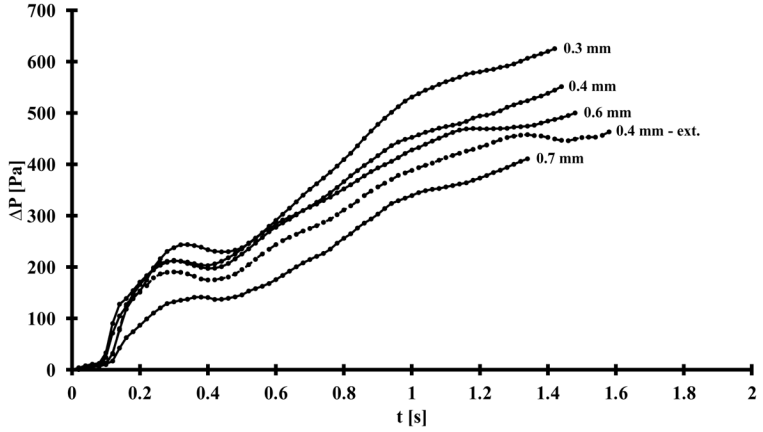

Figure 13: Local pressure drop as a function of a section filling time for several minichannel depths and average flowrate of 3.56 g/s.

the flowrate. It's interesting, that increase of flowrate ten times causes the filling process duration of five times longer (from 1 to 5 s).

It can be seen that in both mentioned cases the curves are visually similar to each other, however, for the flowrate of 0.7 g/s (Fig. 11) there are great differences in details. This did not appear at all for the flowrate of 7 g/s (Fig. 14). In this case the curves are smooth and almost identical qualitatively. Quantitatively, there is, of course, a pressure drop difference. These differences are a result of maldistribution phenomenon presence from

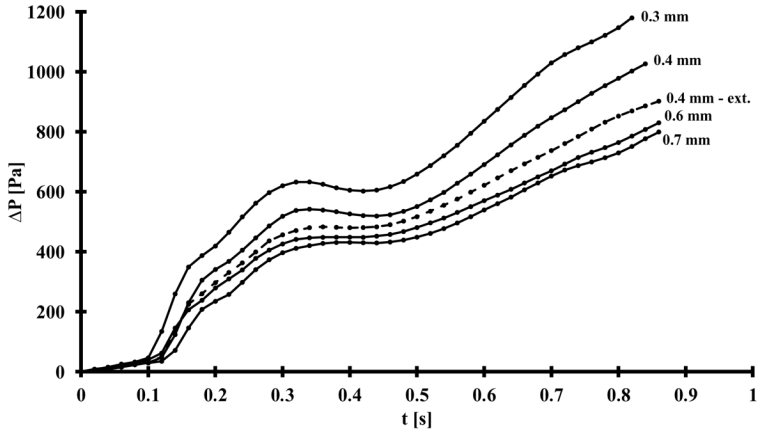

Figure 14: Local pressure drop as a function of a section filling time for several minichannel depths and average flowrate of 7 g/s.

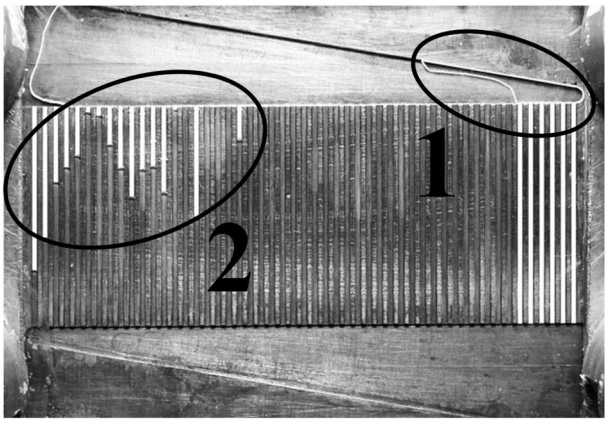

Figure 15: Mechanisms of channels blocking: type 1 – lateral minichannels are blocked through a large bubble of gas phase, trapped in the narrowest part of an outlet manifold; type 2 – the bubbles of gas phase are cut off in individual channels through a forward flow of liquid phase in the outlet manifold.

which the flows at the flowrates of 8.33 g/s are completely free. The authors noticed, that the specifics of the maldistribution process seriously depends on the depth of the minichannels. The two characteristic mechanisms of channel blocking can be distinguished (Fig. 15). They will be present in different proportions and, in some cases, only one of them can occur. Such a process complexity manifests itself in the dynamics of pressure curves. In

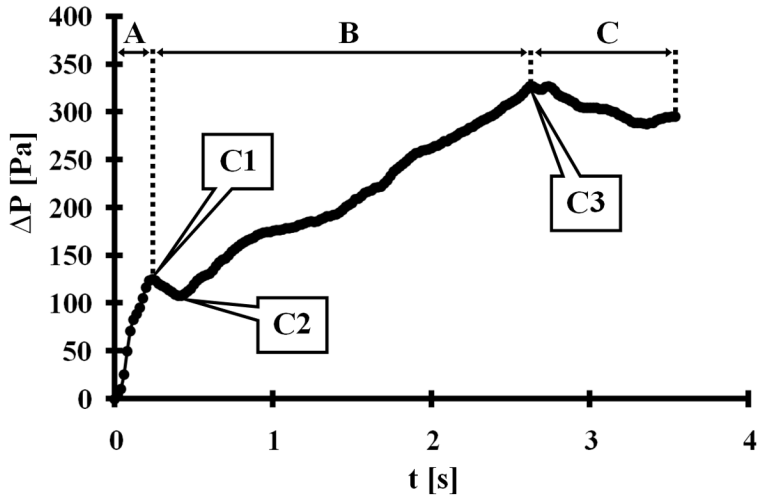

Figure 16: Explanation of characteristic steps of the section filling on the example of minichannels depth of 0.3 mm and flowrate of 0.9 g/s.

extended geometry, the mechanism type 2 may additionally occur wherever the main and transverse channels are intersected, what gives a much more complicated issue.

As can be seen in Fig. 11, the characteristic ranges and critical points can be distinguished on each pressure drop curve. The example has been discussed in detail in Fig. 16. The range 'A' is the stage of flow through the inlet manifold, the range 'B' corresponds to the time when the liquid phase is flowing through the minichannel set, range 'C' is the stage of discharge of the medium through the outlet manifold. The stage 'A' usually has a stable and balanced course because there is little potential for the disorders occurrence. In practice, the only possibility is an incidental air bubble (what is rather the measurement technology imperfection). Because of the difference in depth of inlet manifold and minichannels there is a threshold on which the temporary fluid accumulation occurs before it's entrance to the minichannels. This leads to a local maximum in pressure (C1) which then drops to C2 after breaking up the accumulation. The pressure curve between points C2 and C3 is closely related to the intensity and the character of maldistribution phenomenon. As can be seen in Fig. 11, the differences are significant. For example, in Fig. 16 (minichannel depth of 0.3 mm) the maldistribution phenomenon is poorly visible at flowrate of 0.9 g/s, so the curve in this range is almost linear. For the other depths pressure fluctua-

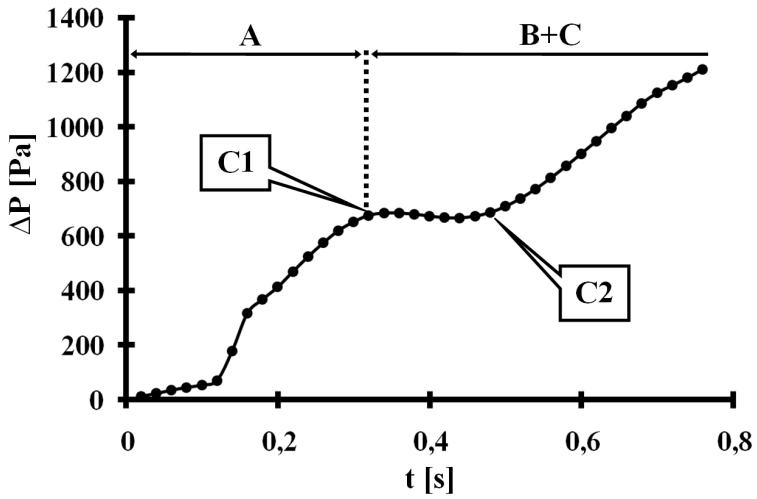

Figure 17: Explanation of characteristic steps of the section filling on the example of minichannels depth 0.3 mm and flowrate of 7.55 g/s.

tions are accordingly higher and the biggest ones are for the case of 0.6 mm. Between the end of the minichannels and the outlet manifold there is also a threshold and the fluid accumulation occurs but, in this case, it takes place in single channels separately and at time intervals so it's effect on pressure change is not so rapid as it was between C1 and C2. Nevertheless, at C3 the fluid starts to flow to the outlet manifold. Fluctuations observed after C3 are related to uneven fluid outflow from the individual minichannels. This unevenness is, of course, directly related to maldistribution intensity, therefore, these fluctuations are the smallest for the section 0.3 mm and the largest for 0.6 mm.

For the case of flowrate 7.55 g/s only C1 and C2 points of a local pressure extremes can be identified (see Fig. 17). Because a further flow distribution between minichannels is almost equal and the maldistribution phenomena did not occur, the pressure curve after C2 is always close to linear. Figure 18 illustrates the characteristic steps of the process. Figure 18A shows the stage of the liquid transition through the inlet manifold. It can be seen, that the working medium creates a front on the line dividing the inlet manifold and the set of minichannels. Figure 18B shows the moment of breaking up the medium accumulation. Then the medium flows through the channels in slightly different order. This corresponds to the area between points C1 and C2 in the Fig. 16 or Fig. 17. Figure 18C shows

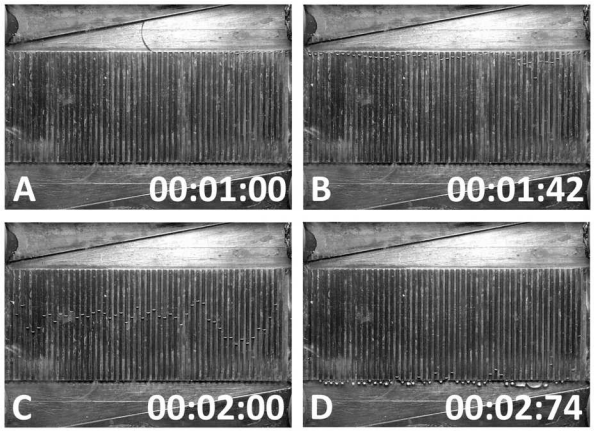

Figure 18: The characteristic steps of the section filling for the minichannels depth of 0.4 mm and flowrate of 1.4 g/s.

a fully developed flow in minichannels according to the profile depending on the individual specification of the section. Figure 18D shows the moment of front formation on the outlet manifold side. It can be seen that regularity is much worse than in the Fig. 18B. This is the equivalent of critical point C3 seen in Fig. 16.

Here it's worth to return to Fig. 4, because that situation needs to be discussed more thoroughly. It is puzzling that in the flowrate range from 1.5 to 8 g/s and for the same dimensions of minichannels the pressure drop is smaller for the extended geometry than for the basic one. It may seem even more surprising because the maldistribution phenomenon in extended geometry occurs in much greater intensity than in the basic (Fig. 19). This can be seen both globally (Fig. 4) and locally (Figs. 20–22), for individual flowrates. This applies not only to local blocking, but also to the main mechanism type 1, which is visible even for flows in the order of 8 g/s for extended geometry.

The first reason is that the introduction of additional channels, although at an angle, increases the cross section of the entire system. The second reason is related to the significant difference between the basic and extended geometry – in the extended variant the liquid has alternative paths to flow out through transverse channels. In this situation, the occurrence of blocking mechanism type 1 does not necessarily eliminate the entire channels within the range of the 'large bubble' of gas phase, but only their

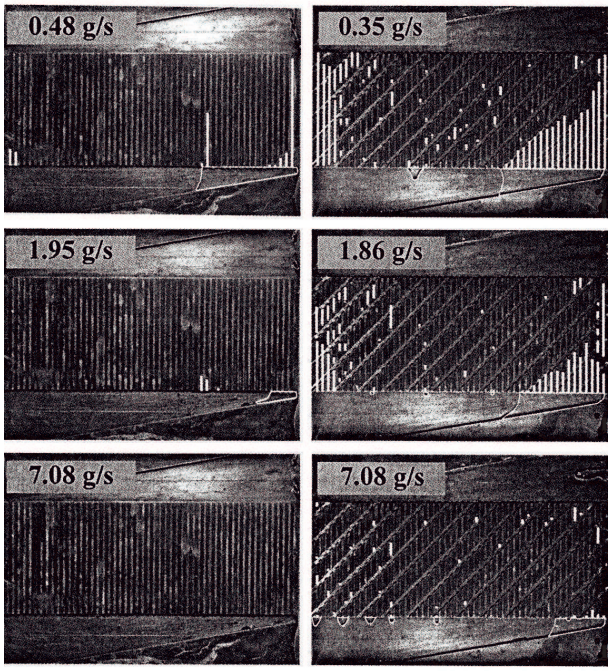

Figure 19: Comparison of channel blocking for the corresponding geometries – 0.4 mm basic and 0.4 mm extended, and for similar flowrates.

Figure 20: Comparison of local pressure drop as a function of a section filling time for basic and extended geometry and for average flowrate of 0.66 g/s.

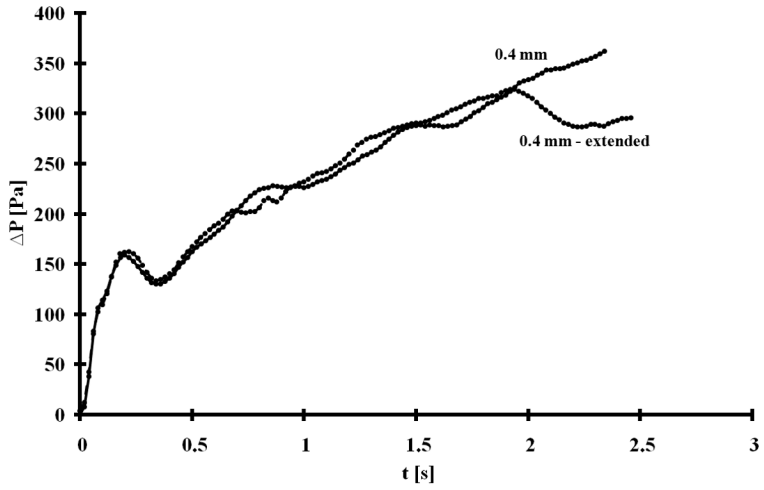

Figure 21: Comparison of local pressure drop as a function of a section filling time for basic and extended geometry and for average flowrate of 1.91 g/s.

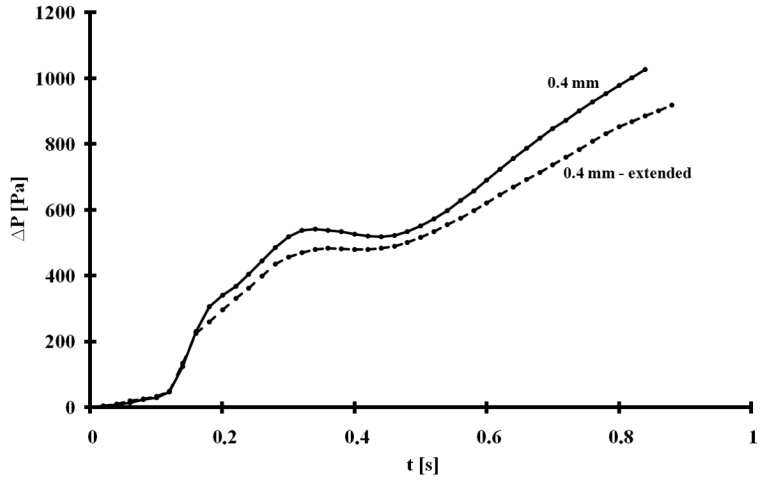

Figure 22: Comparison of local pressure drop as a function of a section filling time for basic and extended geometry and for average flowrate of 7.08 g/s.

corresponding parts. It can be well observed for the example of flowrate 1.95 g/s and 1.86 g/s (Fig. 19). In the basic geometry there is a big bubble characteristic for the blocking mechanism type 1 on the right hand side of the outlet manifold, which completely eliminates all four channels within its range. In extended geometry this bubble is even bigger, but only one

channel (the last) is completely excluded from the work. The remaining channels within the big bubble range can work at least at half of their length because the medium has the ability to alternatively flow through the transverse channels.

6 Conclusions

1. The registered total pressure drop curves are consistent with the flow physics – the pressure drop as a function of mass flow rate increase as the mass flow rate increases. Dependency on minichannels' depth is not strong (in the tested range) – for twice the depth change (from 0.3 to 0.6 mm) the increase in total pressure drop of about 30% can be observed for the flowrate of 7.5 g/s and about 20% for the flowrate of 0.9 g/s. The dependence of pressure drop from the flowrate is strong and it shows a parabolic character. This predisposes minichannel heat exchangers to work with relatively low flowrates in the laminar flow ranges. However, the maldistribution phenomenon should be kept in mind, that occurs and intensifies below a certain critical flowrate value. That means, there are only narrow ranges of flowrates at which a model geometries can work optimally.

2. The registered curves of the local pressure drop show a full qualitative repetition apart of minichannels' depth. The duration of the processes is also comparable. The only difference is strictly quantitative, especially visible for maximum pressures values for the highest flowrates. The nature of these changes overlaps with earlier observations on total pressure drop. It follows that the recorded pressure distributions are the result of more important conditions than just an accidental imperfections of minichannels or the presence of accidental impurities.

3. The introduction of extended geometry causes a further increase in flow resistance at higher flow rates (above 8 g/s). The possible reason for this can be the flow turbulence. However, for the flowrate range from 1.5 to 8 g/s the pressure drop in extended geometry is even smaller, than in a basic one. This is despite the much greater intensification of maldistribution phenomenon. It follows that the benefit of the introduction of extended geometry is not clear. Future research should show whether the improved heat exchange compensates

the intensified problem of maldistribution in the range of acceptable pressure drop.

4. It can be seen that the maldistribution phenomenon is clearly reflected in the course of momentary pressure. For this reason, the analysis of pressure distribution can be a potentially effective method of detecting a maldistribution occurrence and assessing its severity when the visual access to the exchanger interior is not possible. Regardless, the registration of pressure distribution is technically simpler than the visual recording with a quality that allows for a satisfactory evaluation of the phenomenon.

Acknowledgements The work presented in the paper was funded by the National Science Centre research project No. 2015/19/D/ST8/03201 in years 2016–2019. Third Author acknowledges the Polish-Indian Cooperation project between Ministry for Science and Higher Education, Poland and Department of Science and Technology, India (DST/INT/Pol/P-29/2016).

Received 19 April 2018

References

[1] Kays W.M., London A.L.:P *Compact Heat Exchangers, Krieger Publishing Company* 1984. https://books.google.pl/books?id=A08qAQAAMAAJ

[2] Mikielewicz D., Wajs J., Andrzejczyk R., Klugmann M.: *Pressure drop of HFE7000 and HFE7100 during flow condensation in minichannels.* Int. J. Refrig. **68**(2016), 226–241. DOI:10.1016/j.ijrefrig.2016.03.005.

[3] Tuckerman D.B., Pease R.F.W.: *High-performance heat sinking for VLSI.* IEEE Electron Device Lett. **2**(1981), 5, 126–129. DOI:10.1109/EDL.1981.25367.

[4] Teng J.: *Fluid Dynamics in Microchannels.* Intechopen 2012, 403–436. DOI:10.1002/9783527631445.

[5] Mehendale S.S., Jacobi A.M., Shah R.K.: *Fluid flow and heat transfer at micro- and meso-scales with application to heat exchanger design.* Appl. Mech. Rev. **53**(2000), 7, 175–193. http://dx.doi.org/10.1115/1.3097347

[6] Kandlikar S.G., Grande W.J.: *Evolution of microchannel flow passages–thermohydraulic performance and fabrication technology.* Heat Trans. Eng. **24**(2003), 1, 3–17. DOI:10.1080/01457630304040.

[7] Ornatskii A.P., Vinyarskii L.S.: *Heat transfer crisis in a forced flow of underheated water in small-bore tubes.* Teplofiz. Vysok. Temp. **3**(1965), 441–451.

[8] Sturgis J.C., Mudawar I.: *Assessment of CHF enhancement mechanisms in a curved, rectangular channel subjected to concave heating*. J. Heat Transfer. **121**(1999), 2, 394–404. http://dx.doi.org/10.1115/1.2825992.

[9] D.D. Hall, Mudawar I.: *Ultra-high critical heat flux (CHF) for subcooled water flow boiling? II: high-CHF database and design equations*. Int. J. Heat Mass Tran. **42**(1999), 8, 1429–1456. DOI:10.1016/S0017-9310(98)00242-7.

[10] Mikielewicz D., Mikielewicz J.: *A thermodynamic criterion for selection of working fluid for subcritical and supercritical domestic micro CHP*. Appl. Therm. Eng. **30**(2010), 16, 2357–2362. DOI:10.1016/j.applthermaleng.2010.05.035.

[11] Nacke R., Northcutt B., Mudawar I.: *Theory and experimental validation of cross-flow micro-channel heat exchanger module with reference to high Mach aircraft gas turbine engines*. Int. J. Heat Mass Tran. **54**(2011), 5–6, 1224–1235. DOI:10.1016/j.ijheatmasstransfer.2010.10.028. Elsevier

[12] Bahiraei M., Heshmatian S.: *Application of a novel biological nanofluid in a liquid block heat sink for cooling of an electronic processor: Thermal performance and irreversibility considerations*. Energy Convers. Manag. **149**(2017), 155–167. DOI:10.1016/j.enconman.2017.07.020.

[13] Ramos-Alvarado B., Feng B., Peterson G.P.: *Comparison and optimization of single-phase liquid cooling devices for the heat dissipation of high-power LED arrays*. Appl. Therm. Eng. **59**(2013), 1–2, 648–659. DOI:10.1016/j.applthermaleng.2013.06.036.

[14] Jajja S.A., Ali W., Ali H.M., Ali A.M.: *Water cooled minichannel heat sinks for microprocessor cooling: Effect of fin spacing*. Appl. Therm. Eng. **64**(2014), 1–2, 76–82. DOI:10.1016/j.applthermaleng.2013.12.007.

[15] Najim M., Feddaoui M.B.: *New cooling approach using successive evaporation and condensation of a liquid film inside a vertical mini-channel*. Int. J. Heat Mass Tran. **122**(2018), 895–912. DOI:10.1016/j.ijheatmasstransfer.2018.02.034.

[16] Brutin D., Ajaev V.S., Tadrist L.: *Pressure drop and void fraction during flow boiling in rectangular minichannels in weightlessness*. Appl. Therm. Eng. **51**(2013), 1–2, 1317–1327. DOI:10.1016/j.applthermaleng.2012.11.017.

[17] Zhou J., Zhao X., Ma X., Du Z., Fan Y., Cheng Y., Zhang X.: *Clear-days operational performance of a hybrid experimental space heating system employing the novel mini-channel solar thermal & PV/T panels and a heat pump*. Sol. Energy. **155**(2017), 464–477. DOI:10.1016/j.solener.2017.06.056.

[18] Robles A., Duong V., Martin A.J., Guadarrama J.L., Diaz G.: *Aluminum minichannel solar water heater performance under year-round weather conditions*. Sol. Energy. **110**(2014), 356–364. DOI:10.1016/j.solener.2014.09.031.

[19] Sakamatapan K., Wongwises S.: *Pressure drop during condensation of R134a flowing inside a multiport minichannel*. Int. J. Heat Mass Tran. **75**(2014), 31–39. DOI:https://doi.org/10.1016/j.ijheatmasstransfer.2014.02.071.

[20] JY R., LY L., XS D., RR W., WL P., WM T.: *Numerical investigations on characteristics of methane catalytic combustion in micro-channels with a concave or convex wall cavity*. Energ. Convers. Manage. **97**(2015), 188–195. DOI:10.1016/j.enconman.2015.03.058.

[21] Berthier J., Brakke K.A., Furlani E.P., Karampelas I.H., Poher V., Gosselin D., Cubizolles M., Pouteau P.: *Whole blood spontaneous capillary flow in narrow V-groove microchannels*. Sensors Actuators, B Chem. **206**(2015), 258–267. DOI:10.1016/j.snb.2014.09.040.

[22] Zhou P., Tarlet D., Wei M., Fan Y., Luo L.: *Novel multi-scale parallel mini-channel contactor for monodisperse water-in-oil emulsification*. Chem. Eng. Res. Des. **121**(2017), 233–244. DOI:10.1016/j.cherd.2017.03.010.

[23] Illán-Gómez F., García-Cascales J.R., Hidalgo-Mompeán F., López-Belchí A.: *Experimental assessment of the replacement of a conventional fin-and-tube condenser by a minichannel heat exchanger in an air/water chiller for residential air conditioning*. Energy Build. **144**(2017), 104–116. DOI:10.1016/j.enbuild.2017.03.041.

[24] García-Cascales J.R., Illán-Gómez F., Hidalgo-Mompeán F., Ramírez-Rivera F.A., Ramírez-Basalo M.A.: *Performance comparison of an air/water heat pump using a minichannel coil as evaporator in replacement of a fin-and-tube heat exchanger*. Int. J. Refrig. **74**(2017), 558–573. DOI:10.1016/j.ijrefrig.2016.11.018.

[25] W. Zhou, W. Deng, L. Lu, J. Zhang, L. Qin, S. Ma, Y. Tang: *Laser micro-milling of microchannel on copper sheet as catalyst support used in microreactor for hydrogen production*. Int. J. Hydrogen Energy **39**(2014), 4884–4894. DOI:10.1016/j.ijhydene.2014.01.041.

[26] Kandlikar S.G.: *High Flux Heat Removal with Microchannels — A Roadmap of Challenges and Opportunities*. Heat Transfer Eng. **26**(2005), 8, 5–14. DOI:10.1080/01457630591003655.

[27] Qu W., Mudawar I.: *Measurement and prediction of pressure drop in two-phase micro-channel heat sinks*. Int. J. Heat Mass Tran. **46**(2003), 15, 2737–2753. DOI:10.1016/S0017-9310(03)00044-9.

[28] Motyliński K., Kupecki J.: *Modeling the dynamic operation of a small fin plate heat exchanger – Parametric analysis*. Arch. Thermodyn. **36**(2015), 3, 85–103. DOI:10.1515/aoter-2015-0023.

[29] Kupecki J., Badyda K.: *Mathematical model of a plate fin heat exchanger operating under solid oxide fuel cell working conditions*. Arch. Thermodyn. **34**(2013), 4, 3–21. DOI:10.2478/aoter-2013-0026.

[30] Wajs J., Mikielewicz D., Fornalik-Wajs E.: *Thermal performance of a prototype plate heat exchanger with minichannels under boiling conditions*. J. Phys. Conf. Ser. **745**(2016), 032063. DOI:10.1088/1742-6596/745/3/032063.

[31] Mikielewicz D., Wajs J.: *Possibilities of Heat Transfer Augmentation in Heat Exchangers with Minichannels for Marine Applications*. Pol. Marit. Res. **24**(2017), s1, 133–140. DOI:10.1515/pomr-2017-0031.